v. 2, n. 2, 2022

Journal of
Engineering
Research

STUDY AND EVALUATION OF NANOSTRUCTURED β-$AgVO_3$ AS AN INACTIVATOR OF MICROORGANISMS

Maria Tereza Fabbro
https://orcid.org/0000-0002-1261-5817

Luís Presley Serejo dos Santos
https://orcid.org/0000-0003-0531-0983

Vinícius Matteus Ferreira e Santos
https://orcid.org/0000-0003-2195-6362

Felipe de Moraes Yamamoto
http://orcid.org/0000-0002-4625-9224

Jorge Tadao Matsushima
https://orcid.org/0000-0002-3395-3604

Maurício Ribeiro Baldan
https://orcid.org/0000-0001-7605-1064

All content in this magazine is licensed under a Creative Commons Attribution License. Attribution-Non-Commercial-Non-Derivatives 4.0 International (CC BY-NC-ND 4.0).

Abstract: Silver vanadium oxide-based materials, such as $AgVO_3$, have attracted much interest due to their technological applications in sensors, electrical and antibacterial agents, implantable medical devices, and photocatalysts. In this work, the β-$AgVO_3$ nanowires were synthesized by the conventional hydrothermal method at 120 ºC for 48 hours and an effective microwave-assisted way at 120 ºC for 8, 16, and 32 minutes. The phase compositions, structures, and morphologies were investigated by X-ray diffraction (XRD), Spectroscopy Raman (SR), Scanning Electron Microscopy (SEM), and Transmission electron microscopy (TEM) with Energy Dispersive Spectroscopy (EDS) for comparison between both methods. The results reveal a monoclinic structure and the growth of Ag nanoparticles on the surfaces of β-$AgVO_3$ nanowires during electron beam irradiation. Furthermore, it reports that the use of β-$AgVO_3$ nanowires can be used as an inhibitory material for microorganisms.
Keywords: Silver vanadium oxide, microwave-assisted, hydrothermal, microorganism inactivator.

INTRODUCTION

Nanomaterials based on silver vanadium oxides, such as $AgVO_3$, $Ag_2V_4O_{11}$, Ag_3VO_4, and $Ag_2V_2O_7$, have attracted attention for their properties and potential applications like sensors (Mai *et al.*, 2010)6 V for Au contacts, electrodes for lithium-ion batteries (Chen *et al.*, 2008), antibacterial agents (Holtz *et al.*, 2010) or photocatalysts (Xu *et al.*, 2009). For example, β-$AgVO_3$ has been demonstrated to be efficient photocatalysts under visible light irradiation due to its visual light absorption capacity, favorable morphology, and nanocrystalline nature (Hu, Hu e Qu, 2008). An effective strategy to enhance the photocatalytic activity for photocatalysts is to prepare nanostructured architectures with different dimensions nanomaterials, owing to their unique size- or shape-dependent physicochemical properties.

In this context, several methods have been used to prepare $AgVO_3$ nanostructures with different morphologies (Bao *et al.*, 2007; Song *et al.*, 2009; Wang *et al.*, 2015; Xu *et al.*, 2012; Zhang *et al.*, 2006). The conventional hydrothermal method is one of the most extensive methods to prepare nanomaterials with different morphologies and shapes. In the last years, hydrothermal synthesis methods have been combined with microwaves, and this synthesis method is known as the microwave-assisted hydrothermal method (MAH). Therefore, they can create new materials with less time, and less energy spent (Oghbaei e Mirzaee, 2010; Thostenson e Chou, 1999).

The photocatalytic activities of these materials were also improved when the photogenerated holes and electrons could be efficiently separated. According to Zhao et al. (Zhao *et al.*, 2015), surface modification such as Ag nanoparticles on surfaces enhances the separation rate of these holes and electrons because Ag nanoparticles have excellent conductivity and strong electron trapping ability.

This work reports the synthesis of b-$AgVO_3$ nanomaterials prepared by the conventional hydrothermal and microwave-assisted hydrothermal methods. The increase *in situ* of Ag nanoparticles was verified using SEM, TEM, and EDS. We also discuss the photocatalytic characteristics and its properties as a microorganism inactivator such as *Candida albicans*, *Staphylococcus aureus,* and *Escherichia coli*.

EXPERIMENTAL DETAILS

PREPARATION OF β-AGVO$_3$ NANOWIRES

β-$AgVO_3$ nanowires were synthesized by the conventional hydrothermal method

at 120 °C for 48 hours and the microwave-assisted hydrothermal method (MAH) at 120 °C for 8, 16, and 32 minutes. Firstly, 1 mmol of Ammonium metavanadate ($NH_4VO_3.5H_2O$; 99.5% purity, Sigma-Aldrich) was dissolved in 50 mL of deionized water (solution 1). 1 mmol of silver nitrate ($AgNO_3$; 99.8% purity, Sigma-Aldrich) was dissolved in 50 mL of deionized water (solution 2). Solution 2 was added dropwise to solution one under vigorous magnetic stirring at room temperature for 10 min. The resulting solution was transferred to a Teflon autoclave for the first method and placed in a conventional hydrothermal system at 120 °C for 48 hours in an electric furnace. For the second method, the resulting solutions involving microwave-assisted hydrothermal were transferred to a Teflon beaker and placed to 120 °C at different times as previously described. The precipitates for both methods were collected by centrifugation, washed several times with deionized water and ethanol, and dried at 80°C for 12 hours.

CHARACTERIZATIONS

The β-$AgVO_3$ nanowires samples were structurally characterized by XRD using an Ultima IV diffractometer (Rigaku) with Cu-Kα radiation (λ = 1.5406 Å) in the 2θ range of 10 – 70° and step size of 0.02° min^{-1}. SR measurements were recorded using a Modular Raman Spectrometer (Horiba-LabRam HR Evolution), with Ar laser excitation at 514 nm. The morphology, microanalysis, and size of the β-$AgVO_3$ nanowires structures were determined by FEG-SEM (Mira3-Tescan), operating at voltages 10 kV and TEM working at 200kV with energy-dispersive spectroscopy (EDS); model Tecnai G2TF20, FEI.

ANTIBACTERIAL AND ANTIFUNGAL ACTIVITIES OF THE SYNTHESIZED β-$AGVO_3$ NANOWIRES

Broth microdilution assay as described by Clinical and Laboratory Standards Institute - CLSI (CLSI, 2008), was used to determine the minimum inhibitory concentration (MIC) to planktonic cells to evaluate the antifungal activity of the synthesized microcrystals. MICs were defined as the concentrations of β-$AgVO_3$ solution at which there was no visible growth. A standard strain of the Gram-negative bacteria *Escherichia coli* (ATCC 8739), the Gram-positive bacteria *Staphylococcus aureus* (ATCC 6538P), and the fungus *Candida albicans* (ATCC 10231) from Adolfo Lutz Institute's Microorganisms Collection Nucleus were used. To prepare the inoculum, *E. coli* e *S. aureus* were streaked onto Plate Count Agar (PCA, Himedia) incubated at 36 °C for 24 h. *C. Albicans* was streaked onto Sabouraud Dextrose Agar (SDA, Himedia, Mumbai, In) and incubated at 30 °C for 48 h. One loopful of each culture was transferred to 10 ml of Nutrient Broth until the turbidity corresponded to 0,5 compared to the McFarland solution (1,5 x 10^6 CFU/mL).

MIC was determined using 0,035g de β-$AgVO_3$ diluted in 100 mL of peptone water 1% (350 ppm), which remained in agitation for 1 h. The other concentrations (175, 87, and 44 ppm) were calculated and completed with peptone water 1% until 20 mL. Not having the microbial growth, a lower concentration of β-$AgVO_3$ (0,0022g of the sample) and dilute in 100 mL of peptone water 1% (22 ppm). The same procedure described was carried for 12, 0.5, and 0.2 ppm concentrations.

Still, under agitation, it was pipetted 5 ml of the corresponding solution of each concentration in the test tube and 50 µL of the suspension 10^6. The bacterial lines were introduced into the shaker at 36 °C, while the fungal lines were at 30 °C for 24h with 180 rpm rotation. *E. coli* and *S. aureus* were plated in PCA and *C. Albicans* in SDA. The microorganisms were incubated according to the ideal growth temperature for 24 until 48 hours.

RESULTS AND DISCUSSION

XRD patterns of β-$AgVO_3$ synthesized by both methods are illustrated in Figure 1. All XRD peaks can be indexed as monoclinic β-$AgVO_3$ (a=18.106 Å, b=3.579 Å, c=8.043 Å, and β=104.44°), which is consistent with the values given by JCPDS card No. 86-1154. No peaks from other phases can be detected. Figure 1a shows the conventional hydrothermal synthesis at 120 °C for 48 hours with well-defined peaks, indicating the crystallinity of the β-$AgVO_3$. Figure 1b shows the synthesis processed by MAH for 8, 16, and 32 minutes. In this method, as the time increases, the peaks become a bit narrower, indicating that the crystalline phase of the β-$AgVO_3$ also formed increases. Furthermore, the samples synthesized by the conventional hydrothermal method present a higher crystallinity level than the MAH method.

The SEM images of β-$AgVO_3$ are shown in Figure 2a-d. It exhibits that the silver vanadate comprises many 1D nanowires with uniform diameters. Figure 2a presents the SEM image of β-$AgVO_3$ nanowires synthesized by the conventional hydrothermal; it is possible to observe that the Ag nanoparticles growth is not significant, and the diameter of the nanowires is bigger than the other samples. Figure 2b-d shows the β-$AgVO_3$ nanowires synthesized by the MAH method at different times as 8 (Figure 2b), 16 (Figure 2c), and 32 minutes (Figure 2d). In these cases, processed by the MAH method, the nanowires tend to decrease their size and the growth of Ag nanoparticles increases.

Figure 3 shows the growth of the silver nanoparticles on the surfaces of the β-$AgVO_3$ nanowires. Through Figures 3a-c, it is possible to see regions developing minor whitish points over the nanowire, indicating the nucleation of silver nanoparticles and their growth. The red arrow indicates one of these regions where the Ag nanoparticle is already nucleated, and then as time passes, the growth process occurs. This phenomenon is proved in Figure 3c (corresponding to 5 minutes), which shows more significant nanoparticles than Figure 3a (corresponding to 0 minutes). This nucleation and growth occur as soon as the electron beam irradiation reaches a sample.

According to Longo et al. (Longo *et al.*, 2014), the formation of these Ag nanoparticles leads to defects such as silver and oxygens

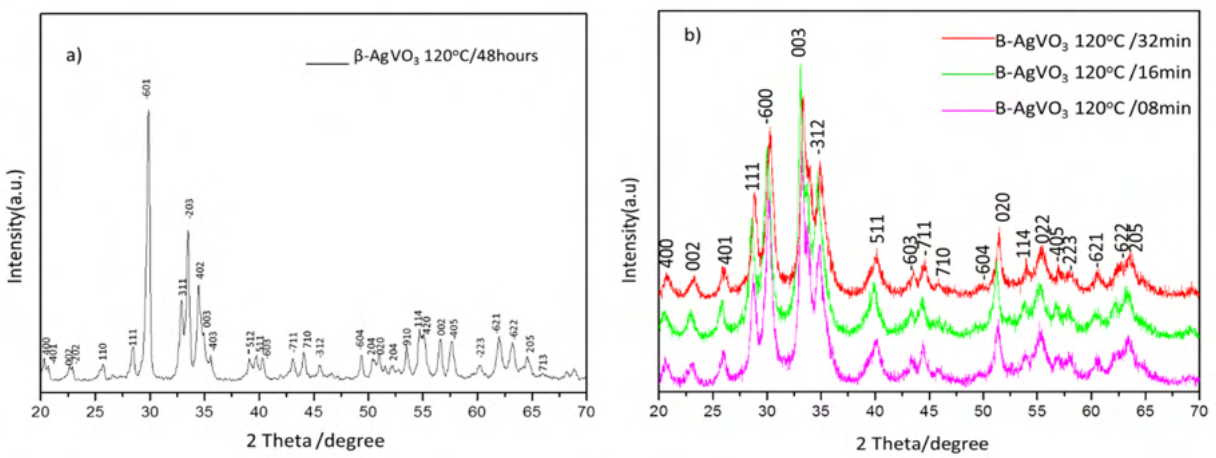

Figure 1. XRD pattern of β-$AgVO_3$ synthesized (a) by the conventional hydrothermal method at 120 °C for 48 hours and (b) by the MAH method at 120 °C for 8, 16, and 32 minutes.

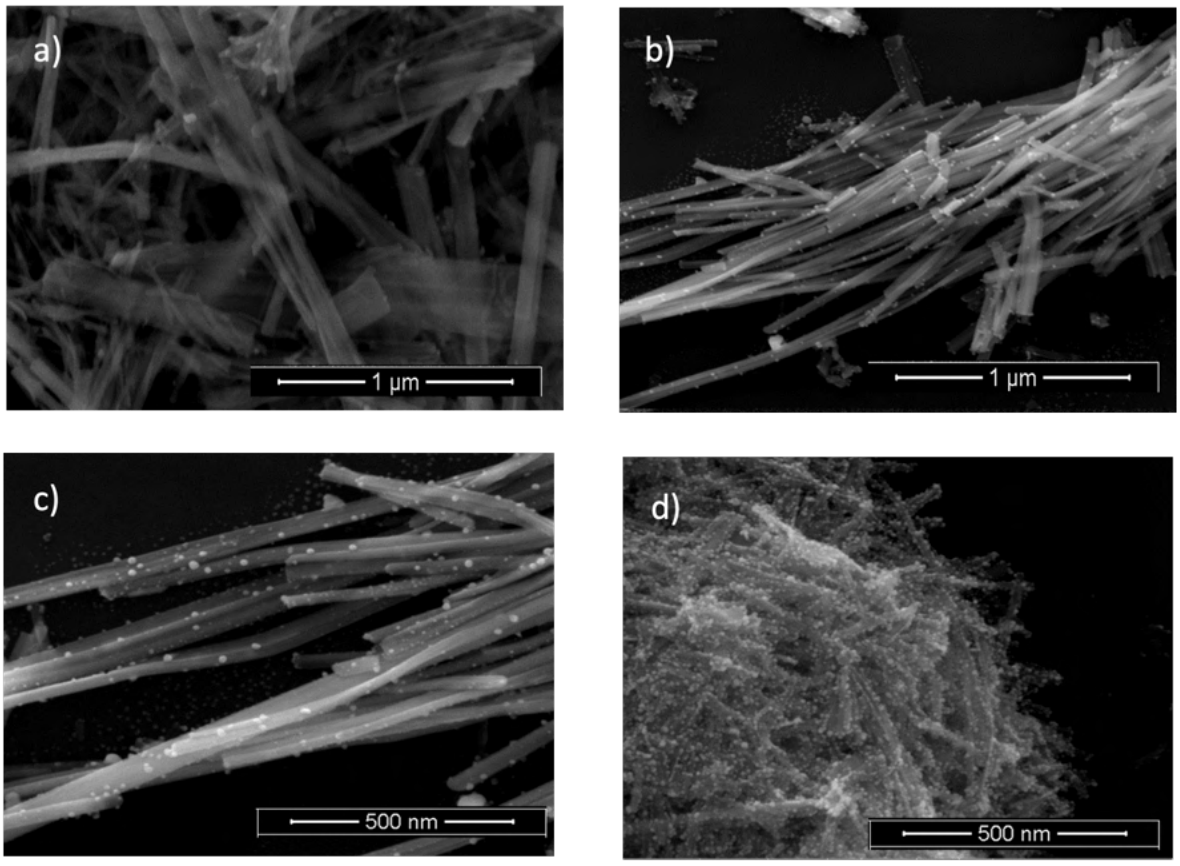

Figure 2. SEM micrographs of the β-$AgVO_3$ nanowires (a) hydrothermal conventional 120 of/48 hours, (b) MAH 120 of/8min, (c) MAH 120 of/16min and (c) MAH 120 of /32min.

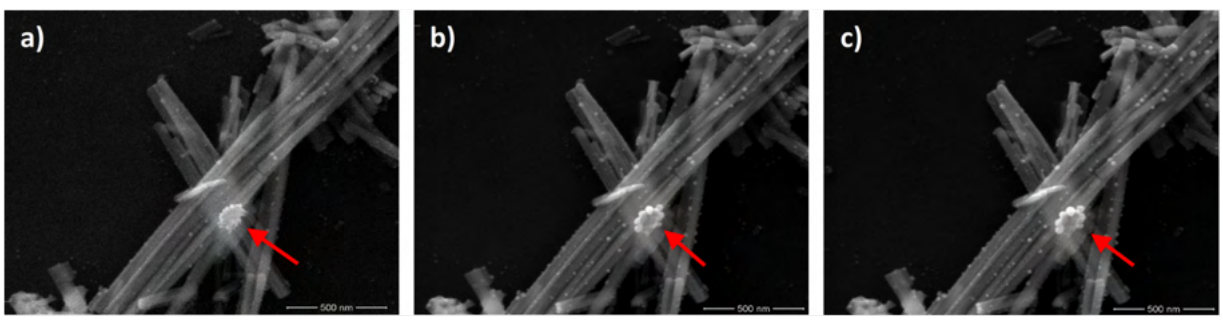

Figure 3. Ag nanoparticles growth on SEM micrographs of the β-$AgVO_3$ nanowires on sample synthesized by the MAH method 120 °C/16min. The red arrow indicates one region where the Ag nanoparticle growth occurs.

vacancies in the β-$AgVO_3$ nanowires. The material presents an n-type semiconductor. As soon as the electron irradiation reaches the bulk of material, the electrons are absorbed by the matrix, which induces the formation of Ag vacancies and transforms a specific region into a p-type semiconductor. The nanoparticles grow as the Ag vacancies concentration increases (as the electrons from the electron irradiation are absorbed). The bigger the concentration of Ag vacancies, the bigger the Ag nanoparticles on the material surface.

All samples synthesized by the MAH method presented a slight growth of Ag nanoparticles. However, the Ag nanoparticles growth is not visible in the sample synthesized by the conventional hydrothermal. This behavior can be associated with the more organized structure of the material synthesized by the traditional hydrothermal, according to the XRD and the SR measurements, which presented a bit more ordered structure at a long and short-range than the MAH method.

Figure 4 shows the TEM images carried out for the β-$AgVO_3$ nanowires synthesized in the microwave-assisted hydrothermal at 120 ^oC for 32 min. Figure 4b corresponds to the red region marked in Figure 4a zoomed. The composition of the areas highlighted in Figure 4b is shown in Figure 5 a-c. Figure 5a exhibit the EDS of region 1, located in the tip of a nanoparticle that nucleated in the material surface (see Figure 4b). This nanoparticle presents 100% of Ag composition, which indicates that it corresponds to a silver nanoparticle. It was expected, and it proves that silver nanoparticles nucleation and growth phenomenon on the material surface, as described in the literature for several materials as the Ag_2WO_4 (Andrés *et al.*, 2014), Ag_2MoO_4 (Andrés *et al.*, 2015), and Ag_2CrO_4 (Fabbro *et al.*, 2016). Figure 5b indicates the analysis conducted on the interface between the nanoparticle and the nanowire located in region 2 (see Figure 4b), and it shows the presence of Ag, V, and O. And, as expected, Figure 5c corresponds to the region 3 (see Figure 4b) carried in the center of the nanowire. It is possible to notice the similarity of the EDS measurements by the presence of Ag, V, and O.

The Raman spectrum of β-$AgVO_3$ nanowires, synthesized by the conventional hydrothermal method, is shown in Figure 6a, and the Raman spectrum of the MAH method is shown in Figure 6b. All the Raman bands are well-matched with that reported for $AgVO_3$ by hydrothermal processes (Holtz *et al.*, 2012). For the sample held in conventional hydrothermal (Figure 6a), the strong band at 886 cm^{-1} originates either from bridging V-O-Ag or from O-V-O vibrations. The 934 cm^{-1} is attributed to symmetric stretching of the VO_4 (Bao *et al.*, 2007). The bands at 844, 807, 731, and 518 cm^{-1} can be assigned to the stretching vibrations of VO_3 groups in the $(V_2O_7)^{4-}$ ion, Ag-O-Ag bridges, and V-O-V bond, corresponding to the asymmetric and symmetric stretches, respectively (Baran, 1997). The bands at 632,477 and 444 cm^{-1} are attributed to the stretching vibration of oxygen shared by two vanadium (V-O-V) fields (Holtz *et al.*, 2012; Liang *et al.*, 2012). Bending vibration of VO_4^{3-} was observed by the presence of the Raman band at 338 cm^{-1} (Sivakumar *et al.*, 2015). The vibrational modes 702, 391, 282, 246, 171, and 132 belong to the VO_4^{3-} (Hardcastle e Wachs, 1991) BiVO4, α-Zn3(VO4. For the sample held in the MAH method (Figure 6b), the Raman modes vibration are well approximated with the modes of the conventional hydrothermal method. The Raman active modes present higher intensities (Figure 6a) compared to the MAH method (Figure 6b), which may be due to the improved surface effects sample β-$AgVO_3$ (Tong *et al.*, 2008) performed by the conventional hydrothermal procedure.

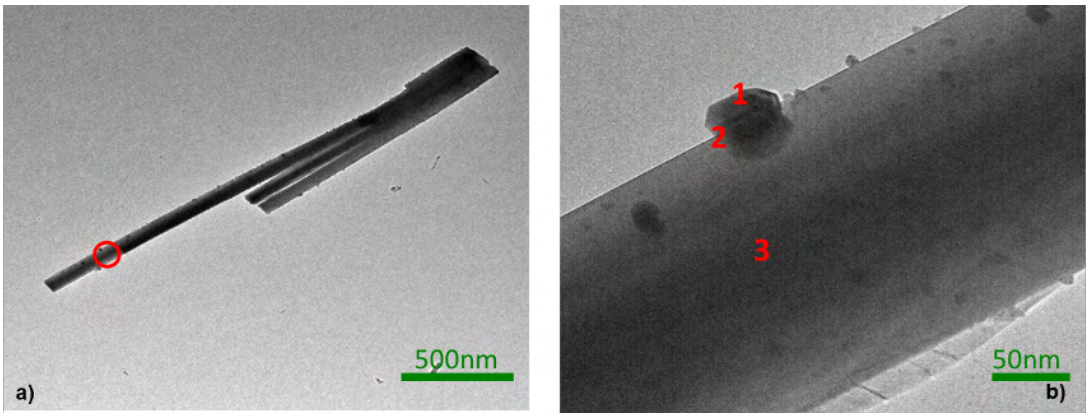

Figure 4. TEM image of the β-$AgVO_3$ nanowires microwave assisted in hydrothermal 120°C/32min.

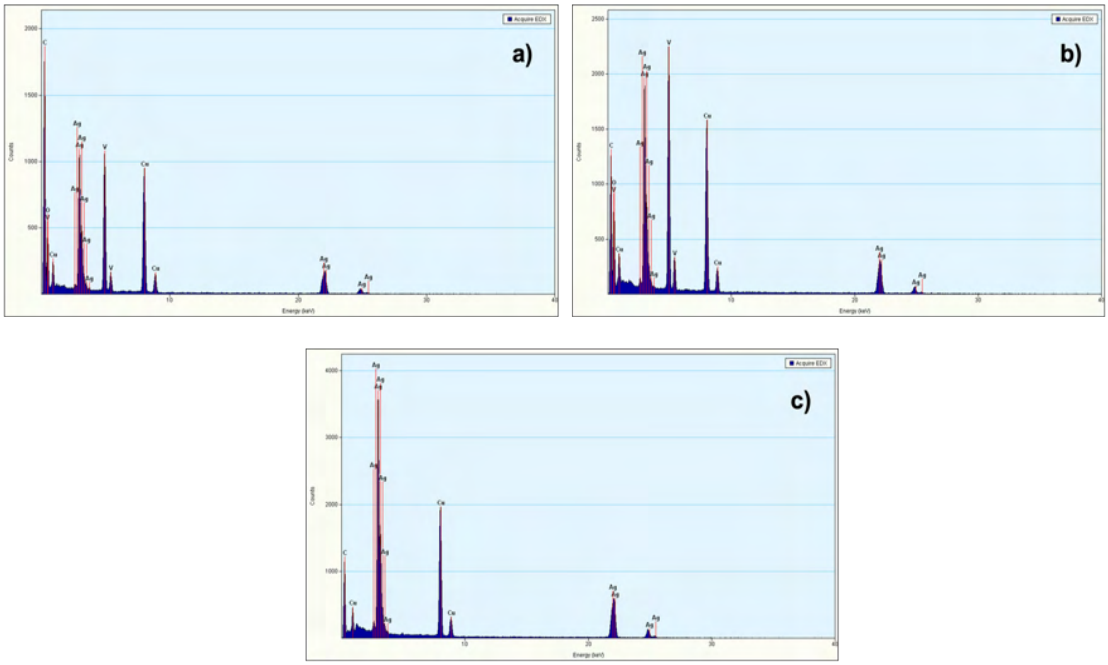

Figure 5. EDS analysis of regions corresponding to Figure 4b (a) region 1, (b) region 2 and (c) region 3. The sample was synthesized by the MAH procedure 120 °C/32 min.

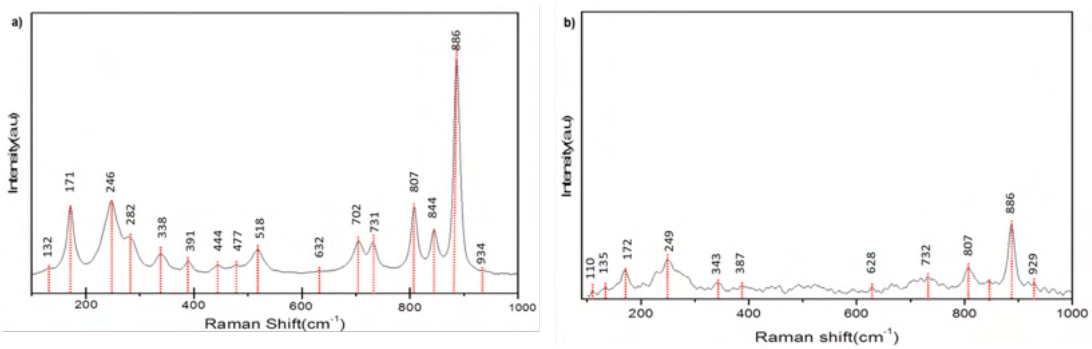

Figure 6. Actives Raman modes spectrum β-$AgVO_3$ nanowires of (a) conventional hydrothermal 120 °C/48 hours and (b) microwave-assisted in hydrothermal 120 °C/32min.

Strain	MIC (µg/mL)	
	Conventional Hydrothermal	Microwave-Assisted Hydrothermal
E. coli (ATCC 8739)	22	11
S. aureus (ATCC 6538P)	87	22
C. albicans (ATCC 10231)	175	11

Table 1. MIC values for β-$AgVO_3$ nanowires against strains of Gram-positive, Gram-negative bacteria and fungus, synthesized by conventional hydrothermal and MAH (120 °C/32min) methods.

The Raman measurements results show the structural order-disorder of β-$AgVO_3$ material, indicating that the traditional hydrothermal method presented a bit higher structural order at short-range than the MAH method according to its narrower peaks.

The antibacterial and antifungal activity of the β-$AgVO_3$ nanowires were tested against the Gram-negative and Gram-positive bacteria strains *E. coli* and *S. aureus*, and the fungal strain *C. Albicans* for both synthesized methods. The MIC values are shown in Table 1. The results show that the β-$AgVO_3$ nanowires tested presented good MIC values.

An analysis of the results indicates that all samples of the β-$AgVO_3$ nanowires synthesized by the MAH method presented higher efficiency than those synthesized by the conventional hydrothermal method. This higher efficiency is related to the higher concentration of Ag nanoparticles, resulting in better antibacterial and antifungal activity.

The results on the *E. coli* and *S. aureus* can be related to a proposed mechanism that states that silver nanoparticles in contact with the bacterial cell membrane can be oxidized, leading to the formation of silver ions, which inhibit the action of the enzymes responsible for cell metabolism (Morones *et al.*, 2005). The presence of Ag ions generates reactive oxygen species, which damage the cell. The silver has a strong tendency to react with sulfur or phosphorus, constituents of the cell membrane, and the DNA nucleic acids, which are preferred sites for binding silver nanoparticles (Sheel *et al.*, 2008). Changes caused by the interaction of the silver nanoparticles in the bacterial membranes and the DNA bounds will affect the bacterial metabolic processes, particularly cell division, ultimately causing cell death (Morones *et al.*, 2005).

For the fungal strain *C. albicans*, the results on the MAH method are much higher than the result assigned to the conventional hydrothermal method. A similar bacterial mechanism seems to occur on the fungal tests. Kim et al. (Kim *et al.*, 2009) reported a potent antifungal effect of silver nanoparticles against *C. albicans*. The results demonstrate that silver nanoparticles destroy the fungal membrane integrity and inhibit the normal budding process.

So, the presence of silver nanoparticles induces bacterial and fungal death, which can explain the results presented in Table 1. The samples that give more concentration of silver nanoparticles (MAH – 120 °C/32 min) also offer much more antibacterial and antifungal activities than the conventional hydrothermal (less concentration of Ag nanoparticles).

CONCLUSIONS

This work reports the experimental results of comparing the microwave-assisted hydrothermal (MAH) method against the conventional hydrothermal method of β-$AgVO_3$ material. All the XRD patterns

presented no deleterious phases. The traditional hydrothermal method exhibits a more ordered structure than all samples synthesized by the MAH method. Although, in the MAH method, the level of crystallinity increases as time increases. The morphology and the Ag nanoparticle's growth on β-$AgVO_3$ surfaces during electron beam irradiation were measured using an SEM and TEM with EDS capabilities. The images showed that the conventional hydrothermal presented no significant Ag nanoparticles growth and presented bigger nanowires diameter. In the MAH method, as time increases, the diameter decreases, and the number and size of Ag nanoparticles increase. According to the MR measurements, the conventional hydrothermal shows a higher order level than the MAH method analyzed. Also, the results of the antibacterial and antifungal activities showed that samples with a higher concentration of silver nanoparticles present better results, which are the samples synthesized by the microwave-assisted hydrothermal method.

ACKNOWLEDGEMENTS

The authors would like to acknowledge INPE for the infrastructure provided, IFSP – Campus SJC and ICT – UNIFESP.

REFERENCES

ANDRÉS, J. *et al.* Structural and electronic analysis of the atomic scale nucleation of Ag on α-Ag2WO4 induced by electron irradiation. **Scientific Reports**, v. 4, p. 5391, 2014.

___. A Combined Experimental and Theoretical Study on the Formation of Ag Filaments on β-Ag2MoO4 Induced by Electron Irradiation. **Particle and Particle Systems Characterization**, v. 32, n. 6, p. 646–651, 1 jun. 2015.

BAO, Q. *et al.* Lithium Insertion in Channel-Structured β-AgVO3 : In Situ Raman Study and Computer Simulation. **Chemistry of Materials**, v. 19, n. 24, p. 5965–5972, nov. 2007.

BARAN, E. J. Vibrational Spectra of Ba2(VO)2O8. **Journal of Raman Spectroscopy**, v. 28, n. 4, p. 289–291, abr. 1997.

CHEN, Z. *et al.* Lithium insertion in ultra-thin nanobelts of Ag2V4O11/Ag. **Electrochimica Acta**, v. 53, n. 28, p. 8134–8137, 30 nov. 2008.

CLSI. **Reference Method for Broth Dilution Antifungal Susceptibility Testing of Yeasts; Approved Standard**. 3rd. ed. Wayne, PA: Clinical and Laboratory Standards Institute, 2008.

FABBRO, M. T. *et al.* Understanding the formation and growth of Ag nanoparticles on silver chromate induced by electron irradiation in electron microscope: A combined experimental and theoretical study. **Journal of Solid State Chemistry**, v. 239, p. 220–227, 2016.

HARDCASTLE, F. D.; WACHS, I. E. Determination of vanadium-oxygen bond distances and bond orders by Raman spectroscopy. **Journal of Physical Chemistry**, v. 95, n. 13, p. 5031–5041, 1991.

HOLTZ, R. D. *et al.* Development of nanostructured silver vanadates decorated with silver nanoparticles as a novel antibacterial agent. **Nanotechnology**, v. 21, n. 18, p. 185102, 7 maio 2010.

HOLTZ, R. D. *et al.* Nanostructured silver vanadate as a promising antibacterial additive to water-based paints. **Nanomedicine: Nanotechnology, Biology, and Medicine**, v. 8, n. 6, p. 935–940, ago. 2012.

HU, X.; HU, C.; QU, J. Preparation and visible-light activity of silver vanadate for the degradation of pollutants. **Materials Research Bulletin**, v. 43, n. 11, p. 2986–2997, 2008.

KIM, K. J. *et al.* Antifungal activity and mode of action of silver nano-particles on Candida albicans. **BioMetals**, v. 22, n. 2, p. 235–242, abr. 2009.

LIANG, S. *et al.* Facile synthesis of β-AgVO 3 nanorods as cathode for primary lithium batteries. **Materials Letters**, v. 74, p. 176–179, 1 maio 2012.

LONGO, V. M. *et al.* Potentiated electron transference in α-Ag2WO4 microcrystals with Ag nanofilaments as microbial agent. **Journal of Physical Chemistry A**, v. 118, n. 31, p. 5769–5778, 2014.

MAI, L. *et al.* Single β-AgVO3 nanowire H2S sensor. **Nano Letters**, v. 10, n. 7, p. 2604–2608, 14 jul. 2010.

MORONES, J. R. *et al.* The bactericidal effect of silver nanoparticles. **Nanotechnology**, v. 16, n. 10, p. 2346–2353, out. 2005.

OGHBAEI, M.; MIRZAEE, O. Microwave versus conventional sintering: A review of fundamentals, advantages and applications. **Journal of Alloys and Compounds**, v. 494, n. 1, p. 175–189, 2010.

SHEEL, D. W. *et al.* Biocidal Silver and Silver/Titania Composite Films Grown by Chemical Vapour Deposition. **International Journal of Photoenergy**, v. 2008, p. 1–11, 2008.

SIVAKUMAR, V. *et al.* AgVO3 nanorods: Synthesis, characterization and visible light photocatalytic activity. **Solid State Sciences**, v. 39, p. 34–39, 2015.

SONG, J.-M. *et al.* Superlong β-$AgVO_3$ Nanoribbons: High-Yield Synthesis by a Pyridine-Assisted Solution Approach, Their Stability, Electrical and Electrochemical Properties. **ACS Nano**, v. 3, n. 3, p. 653–660, 24 mar. 2009.

THOSTENSON, E. T.; CHOU, T.-W. Microwave processing: fundamentals and applications. **Composites Part A: Applied Science and Manufacturing**, v. 30, n. 9, p. 1055–1071, 1999.

TONG, L. *et al.* Single gold-nanoparticle-enhanced raman scattering of individual single-walled carbon nanotubes via atomic force microscope manipulation. **Journal of Physical Chemistry C**, v. 112, n. 18, p. 7119–7123, 8 maio 2008.

WANG, J. *et al.* One-step SDS-assisted hydrothermal synthesis and photoelectrochemical study of Ag4V2O7 nanorods decorated with Ag nanoparticles. **CrystEngComm**, v. 17, n. 35, p. 6661–6668, 2015.

XU, H. *et al.* Enhanced photocatalytic activity of Ag3VO4 loaded with rare-earth elements under visible-light irradiation. **Industrial and Engineering Chemistry Research**, v. 48, n. 24, p. 10771–10778, 16 dez. 2009.

XU, J. *et al.* Synthesis and visible light photocatalytic activity of β-AgVO 3 nanowires. **Solid State Sciences**, v. 14, n. 4, p. 535–539, 2012.

ZHANG, S. *et al.* Synthesis, Characterization, and Electrochemical Properties of $Ag_2V_4O_{11}$ and $AgVO_3$ 1-D Nano/Microstructures. **The Journal of Physical Chemistry B**, v. 110, n. 49, p. 24855–24863, dez. 2006.

ZHAO, W. *et al.* Facile in-suit synthesis of Ag/AgVO3 one-dimensional hybrid nanoribbons with enhanced performance of plasmonic visible-light photocatalysis. **Applied Catalysis B: Environmental**, v. 163, p. 288–297, 2015.